RSC Advances

ROYAL SOCIETY OF CHEMISTRY

www.rsc.org/advances

Amorphous nanosized Al-Ti-Mn trimetal hydrous oxides: Synthesis, characterization and the enhanced performance in arsenic removal

Dong Nguyen Thanh[a*], Zdeněk Bastl[b], Karla Černá[a], Pavel Ulbrich[c], Jaromír Lederer[a]

[a] Unipetrol Centre of Research and Education, Chempark Litvínov, Záluží – Litvínov, 436 70, Czech Republic

[b] J. Heyrovský Institute of Physical Chemistry, Academy of Science of the Czech Republic, Dolejškova 3, CZ-182 23 Prague 8, Czech Republic

[c] Department of Biochemistry and Microbiology, Institute of Chemical Technology, Technická 5, 166 28 Prague 6, Czech Republic

[*]Corresponding author: Dong Nguyen Thanh

Tel: +420 471122287, Fax: +420 475 212 079, E-mail address: dong.nguyen@unicre.cz

Keywords: As(III) oxidation, trimetal hydrous oxide; nanosized; arsenic; adsorption

Abstract

Arsenite (As(III)) is more toxic and more difficult to remove from water than arsenate (As(V)). There is no simple treatment for direct efficient removal of As(III), and thus pre-oxidation of As(III) to As(V) is always required to achieve acceptable removal rates. However, this leads to a complicated operation, which is not cost-effective. To overcome these disadvantages, we have developed a novel nanosized Al-Ti-Mn trimetal hydrous oxide (ATM) adsorbent material combining the oxidation property of manganese dioxide and the high capacity of aluminium hydrous oxide and titanium hydrous oxide to adsorb As(V). This was done by applying a method based on simultaneous oxidation and precipitation. The adsorbent was characterized by BET surface areas measurement, as well as XRD, TEM, XPS, FTIR and TGA techniques. The characterization provided evidence that the new adsorbent was amorphous, had a relatively high surface area (71 m^2/g) and consisted of aggregates of many nanosized particles. Laboratory experiments were carried out to investigate the adsorption kinetics, the adsorption capacity of the adsorbent and the effect of the pH of the solution on the overall arsenic removal. The results indicated that the ATM adsorbent performed excellently in removing both As(III) and As(V) from water. The maximum adsorption capacities for As(III) and As(V) calculated from the Langmuir model are 202.7 and 146.7 mg/g (pH 7.0), and 193.3 and 158.6 mg/g (pH 5.0), respectively. These values exceed significantly those reported in the literature for other nano-adsorbents. Furthermore, the result of XPS analysis of the adsorbent before and after interaction with As(III) confirmed the oxidation/adsorption mechanism for As(III) uptake by ATM. The comparison of -OH density

(OH/g) in fresh ATM and ATM after adsorption of As(III) and As(V) shows that the number of -OH groups on the adsorbent surface was the key factor affecting its adsorption capacity. The amorphous nanosized Al-Ti-Mn trimetal hydrous oxide is thus a promising adsorbent for both As(III) and As(V) removal because of its excellent performance and simple low-cost synthesis process.

1. Introduction

Arsenic (As) pollution in drinking water and its side effects on human health have raised increasing concern globally over the last decade.[1] More than 150 million people worldwide ingest excessive amounts of arsenic through drinking water contaminated from both natural geogenic and anthropogenic sources.[2] Many highly populated Asian countries like Bangladesh, India, China and Vietnam are known to be affected by high groundwater arsenic concentrations [3]. Unlike organic pollutants, arsenic does not decay, and thus circulates and eventually accumulates within the human body, which may result in a variety of health problems, including various forms of cancer (e.g. skin, lung, and bladder), cardiovascular and peripheral vascular diseases [4, 5]. The International Agency for Research on Cancer (IARC) has classified arsenic as a Class A human carcinogen. Controlled-ingestion studies in humans indicate that both As(III) and As(V) are well absorbed from the gastrointestinal tract [6, 7]. In view of the negative effects of arsenic on humans and the environment, the World Health Organization (WHO) has recommended a limit of 10 μg L^{-1} of arsenic for drinking water, which has been adopted by many nations as a regulatory standard [4]. Arsenic mainly exists in four oxidation states (−III, 0, +III and +V), although the predominant forms of As in soil and water are arsenate (As(V)) and arsenite (As(III)) [8]. Depending on the redox state of the water environment, the valence states of arsenic vary from place to place. Arsenate, As(V), is more prevalent in oxygenated surface waters, while arsenite, As(III), is more likely to occur in anaerobic groundwater [9, 10]. As(III) is more toxic than As(V) and also more difficult to remove from aqueous environments [8, 11-13]. The common strategy for As(III) removal is based on its oxidation to As(V) by various techniques [8, 14-16] . Once oxidized to As (V), arsenic can be removed more easily, e.g. by adsorption [8, 17].

Therefore, developing an economical, effective and reliable treatment technique for arsenic removal from groundwater is critical and has gained considerable attention in recent years. Various treatment techniques such as coagulation/precipitation [18], hybrid process of ion exchange membrane-coagulation [19], adsorption [9, 20] and membrane processes [19] have been developed and employed for arsenic removal. Due to its simplicity, high efficiency and cost-effectiveness, adsorption processes are regarded as the most promising methods and largely used for arsenic removal from water and wastewater [8, 21]. Different adsorbents, including natural and synthetic materials, have been extensively investigated to remove

arsenic from aqueous solutions [8, 22, 23]. Most recently, the development of composite adsorbents containing two or more metal oxides has gained considerable attention [24-27]. Some of the recent results have demonstrated that mixed oxides are more active than single oxide thanks to the synergistic effects between the metals in heterogeneous mixed oxides [24-26]. It is well known that aluminium, titanium and manganese hydroxides exist ubiquitously in natural aquatic systems and play an important role in geochemical cycling of nutrients and contaminants [28-30]. Because of their low cost and environmental friendliness, these oxides are also widely used in water treatment engineering systems as important adsorbents for removing contaminants [15, 31-33]. Recently, it was found that the incorporation of aluminum, titanium or manganese into the adsorbents can significantly improve their adsorption capacity toward arsenic because they have a unique selectivity for polyoxy anions. For instance, Tina Basu *et al*. [34] developed a synthetic bimetallic iron(III)–aluminum(III) oxide (NHIAO) adsorbent, which has a much higher As(V) adsorption capacity than the individual Al and Fe oxide adsorbents. Zhang et al.[35] prepared Fe–Mn binary oxide adsorbent, exhibiting a significant enhancement in both As(V) and As(III) removal. Gupta and Ghosh [17] reported the synthesis and use of an Fe–Ti binary mixed oxide for arsenic adsorption. Li et al. [36] synthesized a Ce–Ti oxide adsorbent with high efficiency in both As(V) and As(III) removal. Kun Wu *et al*. [37] found that an Mn oxide - doped Al oxide prepared in their laboratory had a high adsorption capacity towards arsenite and arsenate as compared to the results of recent published research. It is noteworthy that MnO_2 component in the composite adsorbents FMBO, MNFHO and MODAO [35, 37, 38] plays the role of an oxidant in the As(III) uptake through the following simplified reaction:

$$MnO_2 + H_3AsO_3 + 2H^+ \rightarrow Mn^{2+} + H_3AsO_4 + H_2O \quad (1)$$

In addition, the photocatalyzed oxidation of As(III) on TiO_2 offers an environmentally benign method for arsenic removal [39]. Thus the components significantly improved the performance of other pure metal oxides for As(III) removal. From the published results, it can be confirmed that the physico-chemical properties of multi-metal oxides differ from those of their single component oxides [40]. It is also believed that the differences are the primary reason for the improved adsorption performance of multi-metal oxides and these materials may become promising adsorbents for arsenite oxidation and arsenate adsorption from contaminated waters in water treatment systems. To the best of our knowledge, although the characteristics of arsenic adsorption by single-component Al, Ti or Mn hydrous oxides have been studied and reported [41, 42], there is little information available about the adsorption behavior of the composite of trimetal hydrous oxide. Therefore, the ATM adsorbent was recently developed by a simple chemical co precipitation method in our laboratory and is reported in this study. The effect of various adsorbent characteristics, such as adsorption isotherms, adsorption kinetics and the effect of pH on arsenic adsorption, were investigated in batch experiments. The surface characteristics of this adsorbent were also studied by

FTIR, XPS and TGA to elucidate the mechanisms for arsenite oxidation and arsenate adsorption.

2. Material and methods

2.1. Materials

All chemicals were analytical grade and were used without further purification (Sigma Aldrich). Reaction vessels (glass) were cleaned with 1% HNO_3 and rinsed several times with deionized water before use. As(V) and As(III) stock solution was prepared by dissolving $NaHAsO_4{\cdot}7H_2O$ and $NaAsO_2$ in distilled water, respectively. As(V) and As(III) working solutions were freshly prepared by diluting arsenic stock solutions with $NaNO_3$ solution.

2.2. Synthesis of nanosized ATM

ATM was prepared using the oxidation and coprecipitation method. The main preparation procedure was briefed as follows: potassium permanganate ($KMnO_4$, 0.95 g) was dissolved in 100 mL of deionized water; aluminum nitrate nonahydrate ($Al(NO_3)_3{\cdot}9H_2O$, 8.43 g), manganese sulfate monohydrate ($MnSO_4.xH_2O$, 1.53 g) and titanium oxysulfate ($TiOSO_4.xH_2O$, 7.19 g) were dissolved in another 200 mL of deionized water. Under vigorous magnetic stirring, the mixture solution of $Al(NO_3)_3{\cdot}9H_2O$, $MnSO_4.xH_2O$ and $TiOSO_4.xH_2O$ was added into the $KMnO_4$ solution with simultaneous dropwise addition of 4 M NaOH to keep the solution pH in the range of 7.5-8. After addition, the suspension that formed was continuously stirred for 1 h, aged at room temperature for 12 h, and then washed several times with deionized water. The suspension was then filtered and dried at 105 °C for 24 h. The dry material was crushed and stored in a desiccator for further use. As a reference, a sample containing titanium and manganese was also prepared by a similar process.

2.3. Characterization of nanosized ATM

X-Ray diffraction was performed using a Philips APD 1700, Almelo, using copper Kα radiation. The specific surface area of ATM was measured by nitrogen adsorption using the BET method with a Micromeritics ASAP 2000 (Micromeritics Co., USA) surface area analyzer. The particle size of the adsorbent was determined by a laser particle size analyser (Mastersizer 2000, Malvern Co., UK). Structural characterization was carried out using a Transmission Electron Microscope (JEOL JEM-1010, USA). The point of zero charge (PZC) was measured *via* a slightly modified method described by Kinniburgh *et al*.[43]. FTIR spectra were collected using a Thermo Scientific Nicolet iS10 FT-IR Spectrometer applying the ATR technique. The IR spectra of the original adsorbent and arsenic-loaded adsorbent were obtained as dry samples. All IR measurements were carried out at room temperature. The photoelectron spectra of the samples were measured using an ESCA3 MkII (VG Scientific,

UK) electron spectrometer equipped with a hemispherical electron analyzer operated at constant pass energy of 20 eV and giving an energy resolution, expressed by the FWHM of Au $4f_{7/2}$ line, of 1.2 eV. The binding energy scale was calibrated using Au $4f_{7/2}$ (84.0 eV) and Cu $2p_{3/2}$ (932.6 eV) photoemission lines. The spectra were calibrated by setting C 1s peak belonging to adventitious carbon on the sample surface at the binding energy of 284.8 eV. Al Kα radiation was used for electron excitation. A small amount of powder sample was spread on a clean copper surface. The spectra were recorded at room temperature. The Al 2p, Mn 3p, Mn 2p, Ti 3p, Ti 2p, As 3d, O 1s and C 1s photoelectrons were measured. The electron detection angle was 45^{o} with respect to the macroscopic sample surface. The pressure of residual gases in the analyser chamber during spectra acquisition was 2×10^{-9} mbar. The accuracy of the measured electron energies was ±0.2 eV. The overlapping spectral features were resolved into individual components using the damped non-linear least squares method [44] after subtraction of Shirley background [45] using Gaussian-Lorentzian line shape. Quantification of the elemental concentrations was accomplished by correcting photoelectron peak intensities for their cross-sections [46]. In calculations homogeneous composition of the analyzed layer of the measured sample was assumed. Thermal gravimetric study was performed using a 10 mg sample in an alumina pan by a TG-DTA (Discovery DSC, TA Instruments, Delaware, USA).

2.4. Batch adsorption

Adsorption isotherms, adsorption kinetics and the effect of solution pH on arsenic adsorption were determined in batch adsorption experiments. For adsorption isotherms, the experiments were performed at pH 5.0 and 7.0. The pH of the suspensions was adjusted with 0.1 M of NaOH and/ or HNO_3 during the experiment. Initial arsenic concentration varied from 10 mg/L to 500 mg/L. In each test, 30 mg of ATM were loaded in a 100 mL glass vessel, to which 50 ml of a solution containing differing amounts of arsenic were then added. The vessels were shaken on an orbit shaker at 300 rpm for 24 h at 25 ± 1 °C. Then, all samples were filtered by a 0.45 µm membrane filter and analyzed for arsenic. For the adsorption kinetics experiments, defined amount of As(III) or As(V) stock solution was added in a 1000 ml glass vessel containing 500 ml 0.01 M $NaNO_3$ solution to prepare the initial arsenic concentration of 20 mg/L. The solution pH was adjusted to 7.0 ± 0.1 by adding 0.1 M HNO_3 and/or NaOH and then ATM was added to obtain a 0.3 g/L suspension. The suspension was mixed by magnetic-stirring, and the pH was maintained at 7.0 ± 0.1 throughout the experiment by addition of the acid and base solutions. In the whole process, only several drops of acid or base were added into the solution and the total volume was no more than 0.5 ml, which did not significantly influence the arsenic adsorption. Approximately 20 ml aliquots were taken from the suspension at certain time intervals. The samples were filtered through a 0.45 µm membrane filter and analysed for arsenic.

To investigate the influence of pH on arsenic adsorption, experiments were carried out by adding 30 mg of ATM into 150 mL glass vessels containing 50 ml of 50 mg/L As(III) or As(V) solution. The pH of the solutions was adjusted every four hours with dilute HNO_3 or NaOH solution to designated values during the adsorption process. The equilibrium pH was measured and the supernatant was filtered through a 0.45 μm membrane after the solutions have been mixed for 24 h. Then, the residual arsenic concentration in the supernatants was determined. To evaluate the adsorption mechanism of As(III) and As(V) by FTIR, XPS and TGA techniques, the two solid samples were evaluated by adding 90 mg of ATM into 250 mL glass vessels, containing 150 ml of 300 mg/L As(III) or As(V) solution. Having been shaken for 24h, the suspension was then filtrated and dried. The dry samples were stored and denoted as ATM +As(III) and ATM+As(V).

2.5. Analytical methods

After filtration by a 0.45 μm membrane filter, the concentration of residual arsenic concentrations of all experiments was measured using an inductively coupled plasma atomic emission spectroscopy machine (Agilent 720/725 ICP-OES, Agilent co., Australia). Prior to analysis, the aqueous samples were stored in acid-washed glass vessels. All samples used in our analysis were analysed within 12 h after collection.

3. Results and discussion

3.1. Characterization of ATM

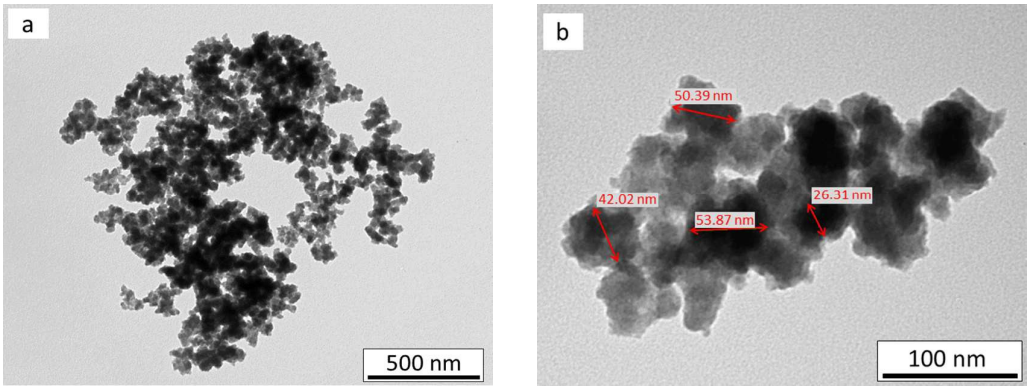

Fig. 1. TEM images of ATM at different magnifications

The X-ray diffraction pattern of the adsorbent is illustrated in Fig. S1a. The XRD spectrum of ATM showed no peaks, which suggested that the co-precipitation process inhibited the formation of any crystalline phase. The distribution of particle size of the powdered ATM is depicted in Fig. S1b, indicating that the average particle size of the trimetal hydrous oxide is 20.76 μm. Fig. 1 a, b illustrates the TEM image of the oxide particles, showing that they are

aggregates formed by small nanoparticles (around 28-53 nm) with no sign of crystallinity. This indicates, in combination with XRD data, that ATM is totally X-ray amorphous. The value of point of zero charge (PZC) of ATM is approximately 3.45. The FTIR, TGA (see section 3.5) and XRD results showed that ATM is X-ray amorphous hydrous oxide of Al, Ti and Mn. The X-ray amorphous ATM has a relatively high BET surface area of 71 m^2/g and a pore volume of 0.329 cm^3/g, in which micropore volume and mesopore volume are 0.0335 cm^3/g and 0.2093 cm^3/g, respectively (Fig. S2 and Fig. S3).

3.2 Adsorption kinetics

The pseudo-first order model and pseudo-second order model were employed to describe the kinetic data. The mathematical representations of the models are given in Eqs. (2) and (3), respectively.

$$\log(q_e - q_t) = \log q_e - \frac{k_1}{2.303} t \quad (2)$$

$$\frac{t}{q_t} = \frac{1}{k_2 q_e^{\,2}} + \frac{t}{q_e} \quad (3)$$

where q_e and q_t are the amount of adsorbed arsenic per unit weight of adsorbent (mg. g^{-1}) in equilibrium and at time *t,* respectively. k_1, is the rate constant of pseudo-first order kinetic adsorption (min^{-1}) as calculated from the gradient of the linear plot of log ($q_e - q_t$) versus t. k_2 is the rate constant of pseudo-second order kinetic adsorption as calculated from the slope of the linear plot of t versus t/q_t. In addition, the initial adsorption rate h can be obtained by the following equation [47]:

$$h = k_2 q_e^{\,2} \quad (4)$$

The gradient and intercept values were obtained by the least-squares regression method. The arsenic adsorption kinetic tests were conducted to determine the adsorption rate.

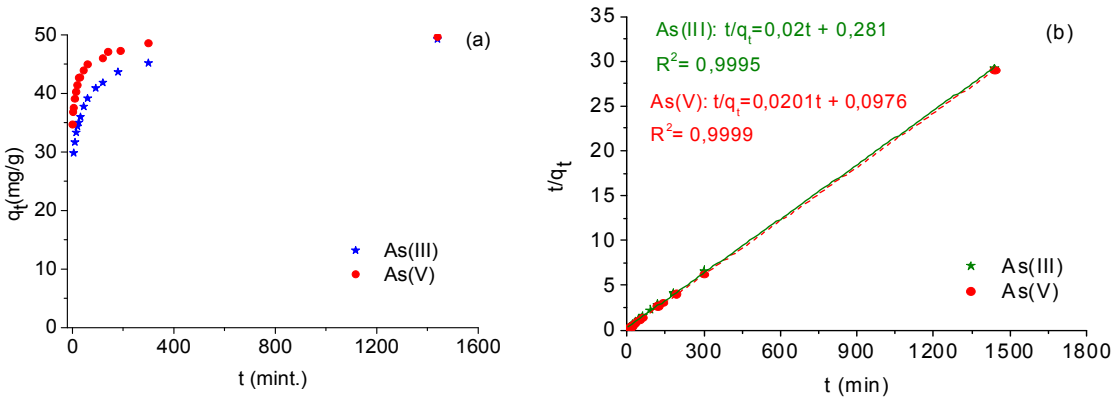

Fig. 2. (a) Adsorption kinetics of As(III) and As(V) on the ATM at pH = 7.0 ± 0.1. Arsenic initial concentrations = 20 mg/L, adsorbent dose = 0.3 g/L and T = 25 ± 1 °C. (b) Pseudo-

second order kinetic model fitting for the removals of As(III) and As(V) by the ATM. The fitted parameters are summarized in Table 1.

Table 1. Adsorption rate constants obtained from pseudo-first order model and pseudo-second order model.

Arsenic species	Pseudo-first order model				Pseudo-second order model		
	q_{exp} (mg/g)	k_1 (min^{-1})	q_e (mg/g)	R^2	q_e (mg/g)	h (mg/g.min)	R^2
As(III)	50.10	0.00299	13.96	0.9579	50.00	3.559	0.9995
As(V)	49.70	0.00230	7.69	0.7324	49.75	10.246	0.9999

Fig. 2a shows the As(III) and As(V) removal kinetic profiles with an adsorbent loading of 0.3 g/L under neutral conditions. The adsorption of As(V) occurred more rapidly and required less time to reach equilibrium than that of As(III). The kinetics parameters were obtained through fitting the experimental data and are summarised in Table 1. According to the values of regression coefficients (R^2), the pseudo-second order model fitted better, which indicates that the adsorption process might be chemisorption (Fig. 2b and Table 1). The initial adsorption rate (h) of As(V) and As(III) onto the ATM was 10.246 and 3.559 mg/g.min, respectively (Table 1). The initial adsorption rate h (mg/g.min) could be used as an indicator of the adsorption rate, especially at the beginning of the adsorption process. It is clear that the initial adsorption rate of As(V) on the adsorbent was higher than that of As(III), indicating that the ATM adsorbent removed As(V) faster than As(III). The relatively slow adsorption rate of As(III) may be caused by the oxidation step before the adsorption of As(V) as evidenced by the XPS results (see section 3.5). In addition, at pH = 7.0 ± 0.1, the dominant As(V) species are negatively charged ($H_2AsO_4^-$ and $HAsO_4^{2-}$), when the dominant As(III) species is neutrally charged (H_3AsO_3). The negatively charged As(V) species are more easily removed than As(III) [48, 49]. The adsorption behavior of As(V) and As(III) on the ATM was similar to that on the adsorbents reported previously, such as iron(III)-tin(IV) binary mixed oxides [50].

3.3 Adsorption isotherms

The arsenic adsorption capacities of the ATM at the two pH values were evaluated using the isotherms and are presented in Fig. 3. It can be seen that the ATM has high adsorption capacity for both As(III) and As(V). For As(V), its adsorption capacity was slightly reduced when the pH of the solution was increased from 5.0 to 7.0. In contrast, in the case of As(III) the increase in pH slightly enhanced its adsorption. In addition, at low initial equilibrium concentration, the adsorbent is more effective in removing As(V) than As(III). For example, the As(III) and As(V) adsorption capacities are 69.7 mg/g and 76.0 mg/g at initial

concentration of 50 mg/L and pH 7.0. However, it has higher adsorption capacity for As(III) than that of As(V) at higher equilibrium concentration. These results indicate that the adsorption of As(III) and As(V) might be dominated by different mechanisms. Both Langmuir and Freundlich models were used to describe the adsorption isotherms. The Langmuir equation and Freundlich equation are represented as Eqs. (5) and (6), respectively.

$$q_e = \frac{q_m K_L C_e}{1 + K_L C_e} \tag{5}$$

$$q_e = K_F C_e^{1/n} \tag{6}$$

where q_e is the amount of arsenic adsorbed on the solid phase (mg/g), C_e is the equilibrium arsenic concentration in solution phase (mg/L), K_L is the equilibrium adsorption constant related to the affinity of binding sites (L/mg), q_m is the maximum amount of the arsenic per unit weight of adsorbent for complete monolayer coverage, K_F is roughly an indicator of the adsorption capacity and n is the heterogeneity factor – the more heterogeneous the surface, the lower the value of the factor.

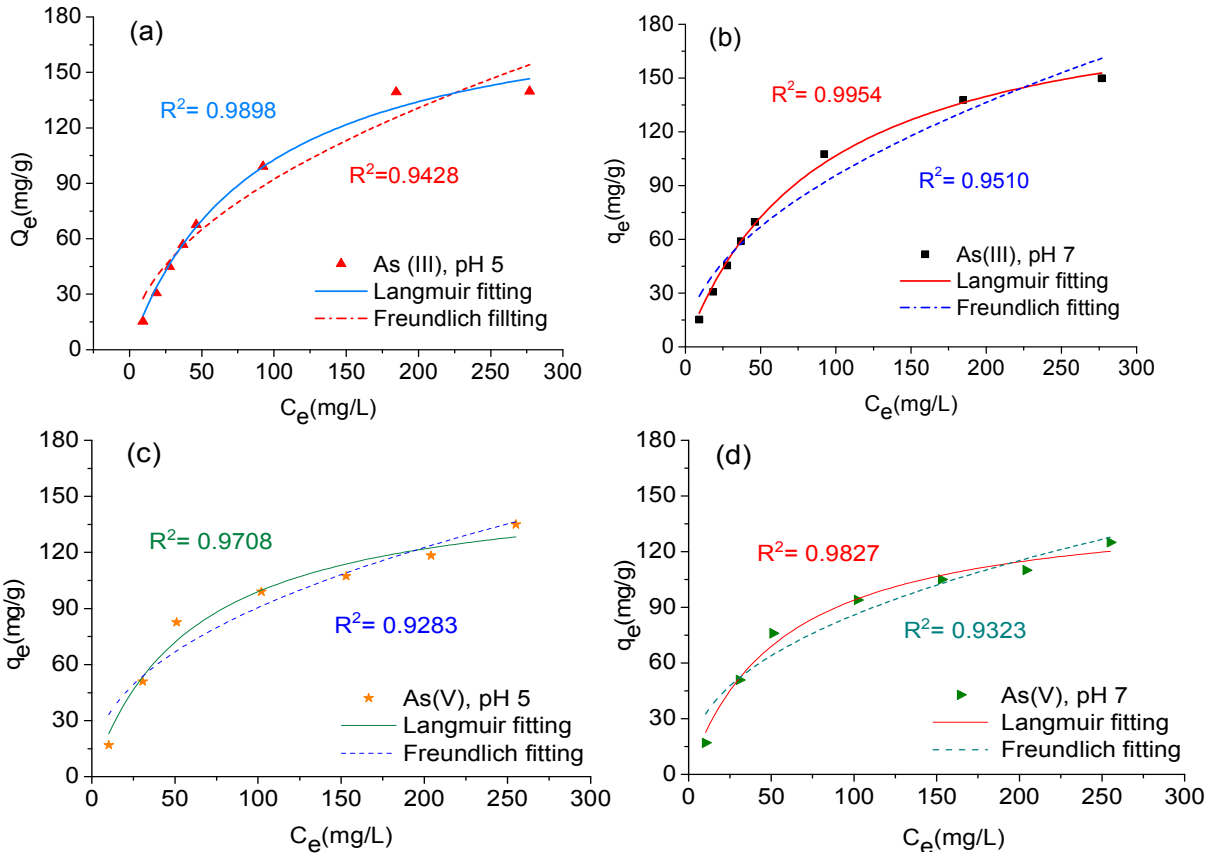

Fig. 3. Adsorption isotherms for (a,b) As(III) and (c,d) As(V) by ATM at pH 5 and pH 7 (T = 25 ± 1 °C; (—) Langmuir model fitting and (----) Freundlich model fitting).

Table 2. Langmuir and Freundlich isotherm parameters for As(III) and As(V) adsorption on ATM at pH 5.0 and pH 7.0.

As species and pH	Langmuir model			Freundlich model		
	q_m (mg/g)	K_L (L/mg)	R^2	K_F (g/L)	n	R^2
As(III), pH 5.0	193.28	0.0113	0.9898	9.00	0.5050	0.9428
As(III), pH 7.0	202.72	0.0111	0.9954	9.05	0.5121	0.9510
As(V), pH 5.0	158.58	0.0166	0.9708	12.00	0.4380	0.9283
As(V), pH 7.0	146.72	0.0177	0.9827	12.14	0.4246	0.9323

The adsorption constants obtained from the isotherms are presented in Table 2. As shown there, the higher regression coefficient suggests that the Langmuir model is more suitable than the Freundlich model for describing how arsenic is adsorbed by ATM. The Langmuir model assumes that adsorption occurs on a homogeneous surface. Interestingly, although ATM consists of aluminum, titanium and manganese hydrous oxides, it exhibited the behavior typical for adsorption of a homogeneous surface having adsorption sites with similar adsorption energies. The maximal adsorption capacities for As(III) and As(V) calculated from Langmuir model are 202.7 and 146.7 mg/g (pH 7.0), and 193.3 and 158.6 mg/g (pH 5.0), respectively.

Table 3. Comparison of maximum arsenic adsorption capacities for different adsorbents.

Adsorbent	As con. range (mg/L)	Max. As(III) adsorption capacity (mg/g)	Max. As(V) adsorption capacity (mg/g)	Reference
MnO_2 nanorods	0-200	19.41	n.a.	[51]
Al_2O_3/$Fe(OH)_3$	0.56–10.1	9.0 (pH 6.6)	36.7 (pH 7.2)	[52]
Nano-TiO_2	0–130	99.0 (pH 7.0)	n.a.	[53]
CuO nanoparticles	0–100	26.9 (pH 8.0)	22.6 (pH 8.0)	[22]
Fe-Ti oxides	5.0–250	85.0 (pH 7.0)	14.3 (pH 7.0)	[54]
Fe–Mn binary oxide	0–40	100.4 (pH 6.9)	53.9 (pH 6.9)	[35]
Mn oxide doped Al oxide	1-90	142.2 (pH 7.0)	99.7 (pH 7.0)	[37]
Fe_3O_4:Cu	1-85	37.97 (pH 5.0)	42.90 (pH 5.0)	[55]
Fe–Zr trimetal oxide	0–40	120.0 (pH 7.0)	46.1 (pH 7.0)	[56]
Al-Ti-Mn trimetal hydrous oxide	0–200	193.3 (pH 5.0)	158.6 (pH 5.0)	This study
Al-Ti-Mn trimetal hydrous oxide	0–200	202.7 (pH 7.0)	146.7 (pH 7.0)	This study

To the best of our knowledge, these values are among the highest adsorption capacities for arsenic reported in literature (Table 3). Such high capacity indicates that the prepared ATM is very effective for both As(III) and As(V) removal.

3.4. The influence of pH on arsenic adsorption

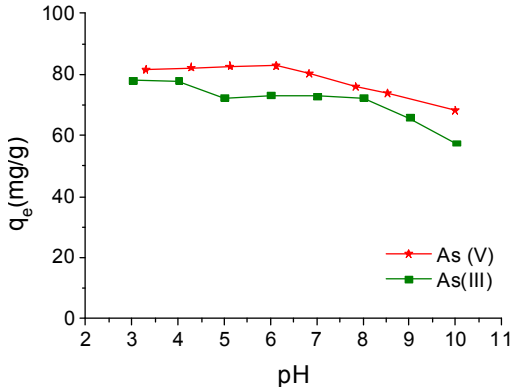

Fig. 4. Effect of solution pH on As(III) and As(V) adsorption by ATM. The initial arsenic concentration = 50 mg/L, adsorbent dose = 0.6 g/L and T = 25 ± 1 °C.

The results in Fig. 4 illustrate the effects of pH on the removal of As(V) and As(III). In case of As(V) adsorption, negligible variation in As(V) capacity was observed in the pH range of 3.3 –6.1, while a further pH increase up to 10 resulted in an obvious drop in As(V) uptake. This phenomenon can be explained by electrostatic and ligand exchange mechanisms. The pH of the solution not only affected the surface charge of the ATM, but also influenced arsenic speciation in solution. In aqueous solutions, $H_2AsO_4^-$ and $HAsO_4^{2-}$ are the dominant As(V) species under the tested pH range (3 –10). The adsorbent had a point of zero charge at pH 3.45, suggesting that the adsorbent surface was negative at pH above 3.45 and positive at pH below 3.45. Lower pH is favorable for the protonation of the adsorbent surface. Increased protonation is thought to enlarge the attraction force existing between the adsorbent surface and anionic arsenic species, and therefore to increase the amount of As(V) adsorbed in the lower pH region. In the higher pH region, the negatively charged sites dominate, the repulsion effect is stronger and the amount of adsorption consequently drops. On the other hand, as illustrated schematically by the reactions given in the Eqs. (7,8) below and by Le Chatelier's principle, when the pH increases, there are more hydroxyl ions (OH^-) present in the solution, which increases the competition for adsorption sites; therefore, the surface adsorption of As(V) is lowered. On the contrary, the reduction of pH facilitates the ligand exchange by adsorption, resulting in increased arsenic removal. Similar phenomena were also observed for the adsorption of arsenic onto other Fe-Mn binary oxides [26] and MnO_2 nanorods [51]. The reason is that the adsorption of strong acid anions by metal oxides and hydroxides typically decreases with an increasing pH [57].

The same trend was observed with the As(III) species. Generally, As(III) adsorption capacity decreases with an increase in pH of the solution. The maximum adsorption of As(III)

occurred under acidic conditions, remained relatively stable at the pH range of 5-8 and decreased markedly with further increase in pH. It was quite different from other adsorbents such as Fe-Zr binary oxide [56] or ZrO_2 nanoparticle [58]. Such different pH dependence implies that As(III) adsorption on ATM adsorbent may be driven by a different mechanism. As illustrated later (section 3.5), As(III) removal by ATM contains two basic processes, oxidation of As(III) to As(V) by Mn-oxidinves and adsorption of As(V) by metal oxides. As shown in Eq. (1), low pH is favorable for As(III) oxidation into As(V) by Mn oxides, while high solution pH resulted in a smaller amount of As(III) oxidized into As(V). On the other hand, after the oxidation process, the increase of solution pH is also unfavorable for removal of As(V) species as described above by electrostatic and ligand exchange mechanism.

In addition, it is necessary to mention that although the adsorption capacity of ATM towards As(III) and As(V) was reduced gradually with the increase in pH, except for the pH range of 5-8, the adsorption capacities remained relatively high and stable, which is different from the other adsorbents reported previously [8, 20, 23, 51]. This behavior has practical implications for determining the adsorbent's usability in the treatment of drinking water.

3.5. Influence of coexisting anions on adsorption

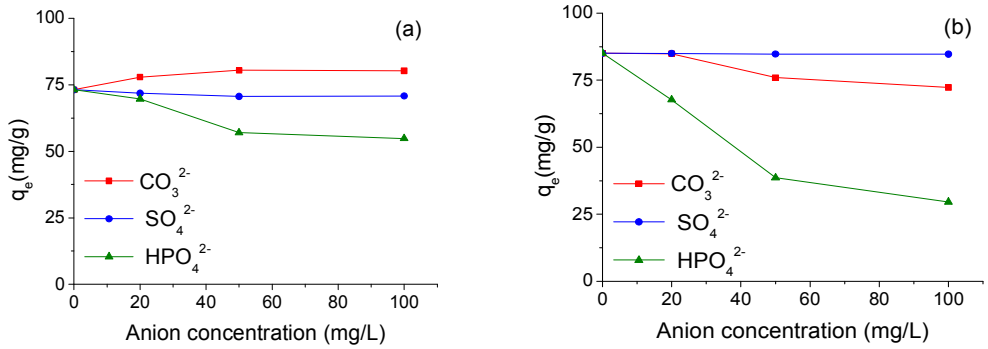

Fig. 5. Effects of co-existing anions on (a) As(III), (b) As(V) adsorption at different concentrations. Initial anion species concentration 50 mg/L, concentration of co-existing anion 20-100 mg/L, adsorbent dose 0.6 g/L and T = 25 ± 1 °C.

The effects of commonly present anions such as CO_3^{2-}, SO_4^{2-} and HPO_4^{2-} in water on arsenic adsorption were examined at different concentrations (from 20 to 100 mg/L). The results are shown in Fig. 5. The presence of HPO_4^{-} hinders significantly the adsorption of both As(III) and As(V); especially at high concentration levels this may be due to a strong competition for the binding sites of the adsorbent between HPO_4^{2-} and arsenic. The presence of CO_3^{2-} and

HPO_4^{2-} increased the pH of the solution (Fig. S7), thus the high concentration of $CO_3^{2-}$and HPO_4^{2-} had a negative effect on As(V) removal since the ATM adsorbent exhibited the highest adsorption capacity at low pH. On contrary, the increase in CO_3^{2-} concentration and the resulting higher pH of the solution facilitated the adsorption of As(III) (Fig 5.a and Fig. S7). It can be hence suggested that the adsorption of As(III) is more sensitive to the change of pH solution than to the effect of coexisting CO_3^{2-} anions. The presence of SO_4^{2-} at different concentrations has only a minor effect on the pH of the solution and on the adsorption capacity.

3.5. Evaluation of the adsorption mechanism by XPS, FTIR and TGA techniques

Table 4. Population of O^{2-} oxygen and –OH groups obtained from fitted XPS spectra of the O 1s peak of the optimized ATM before and after As(III) and As (V) adsorption.

Sample	Peak	FWHM, eV	Percentage, %
ATM	O^{2-}	2.6	52
	OH^-	2.6	48
ATM + As(III)	O^{2-}	2.7	61
	OH^-	2.7	39
ATM + As(V)	O^{2-}	2.5	56
	OH^-	2.5	44

Table 5. Surface hydroxyl (-OH) group determination for ATM, Ti-Mn binary hydrous oxide (TM), ATM after shaking in water and ATM after adsorption of As(III) and As(V). The specific surface area of ATM and TM is 71 and 336 m^2/g, respectively.

Sample	D_{OH} (OH/nm^2)	$OH*10^{20}$(OH/g)
ATM	162.64	125.39
TM	17.39	58.25
ATM + water	145.78	112.39
ATM + As(III)	98.58	76.01
ATM + As(V)	106.96	82.46

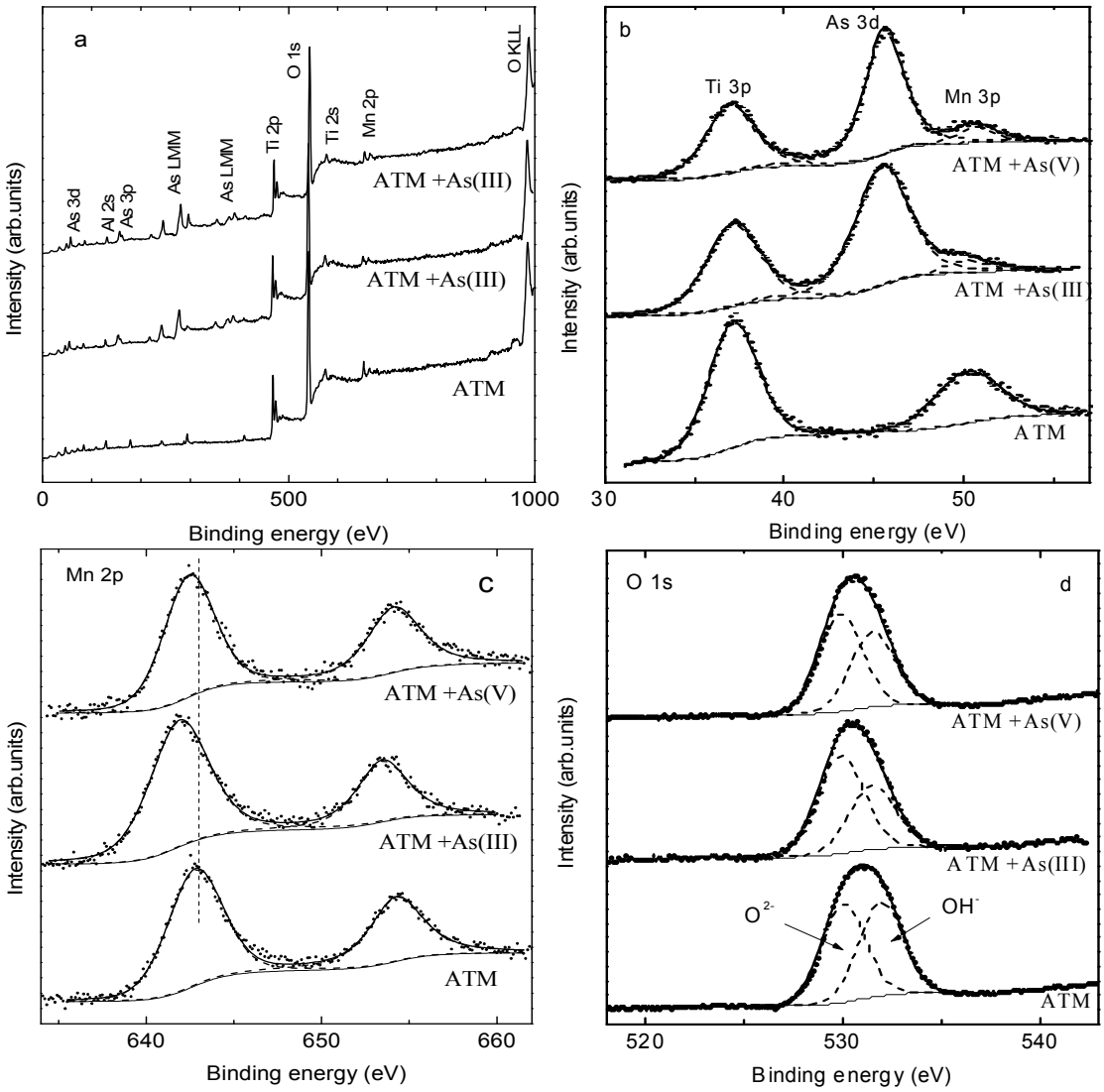

Fig. 6. XPS spectra of ATM, (a) wide scan spectra; (b) spectra of As 3d electrons; (c) spectra of Mn 2p electrons; and (d) spectra of O 1s electrons. (Virgin ATM = ATM, ATM after adsorption of As(III) = (ATM+As(III)) and ATM after adsorption of As(V) = (ATM+As(III)).

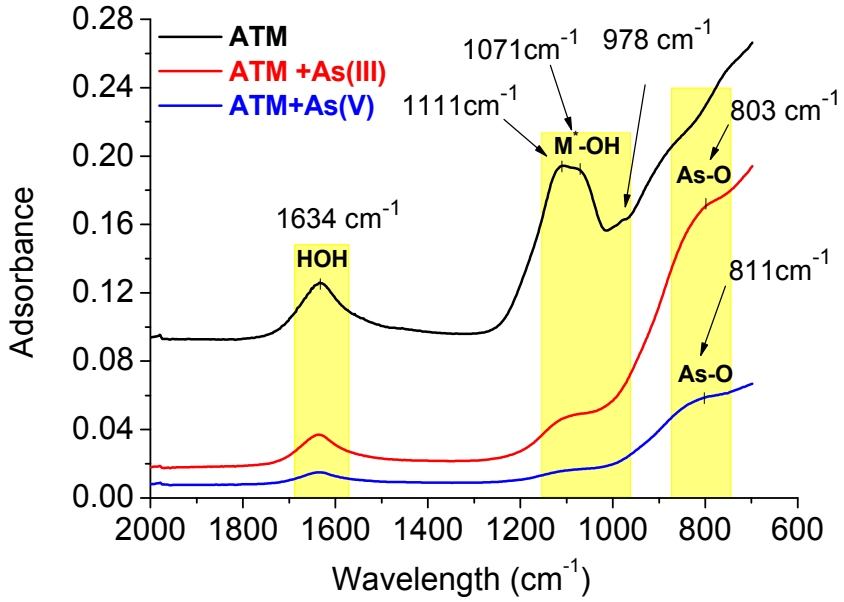

Fig. 7. FTIR spectra of virgin ATM and after interaction with As(III), and As(V), (M*= Al, Ti, Mn)

XPS and FTIR analyses were employed to explore the interactions between As(III), As(V) and the adsorbent surface, and the obtained results are shown in Fig. 6 and Fig. 7. XPS is a useful tool for the determination of concentration and chemical state (i.e. valence) of elements present in the surface layers of the studied samples [59, 60]. As shown in Fig. 6a, the wide scan XPS spectrum of the fresh adsorbent indicates presence of Al, Ti, Mn, C, O and small amounts of S on the adsorbent surface (originated from the precursor metal salt). New As3d core level peak as well as As LMM and As3p peaks appeared in the spectra of ATM after its interaction with As(V) or As(III), indicating clearly the presence of arsenic on the surface of the samples. The elemental concentrations (in atomic %) before and after adsorption calculated from XP spectra are shown in Tab. S1. Fig. 6b illustrates the As3d spectra of the ATM after adsorption of As(III) and As(V). The same binding energy of 45.5 eV is observed for the As3d lines of arsenic loaded ATM regardless of the arsenic state present in the solution. The value is consistent with the values reported [61, 62] for arsenic in oxidation state (+V). Thus, it is inferred that As(III) species were completely oxidized to As(V) on the surface of the ATM. ATM played a role of catalyst for As(III) → As(V) reaction and the Mn-hydrous oxide component might function as the oxidant [9]. As shown in Tab. S2, the binding energies of electrons in Mn(II), Mn(III) and Mn(IV) oxidation states of manganese are close and the spectra of Mn 3p and Mn 2p photoelectrons are rather complex [63, 64]. Consequently,

the population of individual oxidation states from the measured spectra cannot be unequivocally ascertained. The measured binding energy of Mn 3p electrons, 50.2±0.2 eV is within the experimental error not influenced by adsorption of As and corresponds to (IV) oxidation state of manganese [65]. The shift in the Mn $2p_{3/2}$ spectra of about 0.5 eV towards lower binding energy is observed for the ATM+As(III) sample (Fig. 6c). The lower kinetic energy of the Mn $2p_{3/2}$ electrons compared to Mn 3p electrons results in higher surface selectivity of the Mn $2p_{3/2}$ electrons and the observed shift thus indicate presence of Mn (+III) [66, 67] in the uppermost layer of the ATM+ As(III) sample (for MnO_2 and Mn_2O_3 the inelastic mean free path of Mn 3p electrons calculated from the TPP 2M formula [68] is 2.7 nm, while for Mn $2p_{3/2}$ electrons it amounts to 1.8 nm). It was also reported that manganese oxides acted as a catalyst for the oxidation of organic compounds and inorganic ions [9, 69]. The spectra of O 1s photoelectrons (Fig. 6d) consist of two components, one belonging to oxygen in the ATM structure (at 530.2 eV) assigned to O^{2-} and the other pertaining to hydroxyl groups (at 532.1 eV) assigned to OH^- on the surface [70]. The population of -OH groups decreased markedly after adsorption of As(III) and As(V). The details are listed in Table 4. This suggests that –OH groups on the adsorbent surface played an important role in the arsenic adsorption and were replaced by arsenic species.

The FTIR spectrum of ATM has strong hydroxyl stretching (3337 cm^{-1}) and bending (1634 cm^{-1}) vibrations of physically adsorbed H_2O [71, 72] (Fig. 7 and Fig. S4). The bands at 1111, 1071 and 978 cm^{-1} generally correspond to the bending vibration of hydroxyl groups of metal oxides (M*-OH) [26, 73]. After adsorption of As(III) and As(V), the three peaks of hydroxyl groups weakened significantly, and new bands, corresponding to As-O stretching vibration, appeared at 803 cm^{-1} and 811 cm^{-1} for As(III) and As(V) adsorption experiment, respectively [74, 75].

According to Pena *et al*., the values of asymmetric stretching vibrations of (As-O) band position depend on the As(V) species present, which is strongly effected by the pH of the solution, [42] and furthermore the intensity increases with the increase of As(V) concentration. The values ranged from 795 cm^{-1} in AsO_4^{3-} to 909 cm^{-1} in $H_2AsO_4^-$ when the pH was decreased from 12.5 to 5.0 [72]. The corresponding values for adsorbed As(V) species were reported: 820 cm^{-1} [76], 828 cm^{-1} [71], and 836 cm^{-1} [72] for the adsorption of As(V) on Fe–Mn oxide nanoparticles, Ce(IV)-doped iron oxide and Fe-Ce bimetal oxide, respectively. The shift of the band positions was attributed to a change in symmetry or asymmetry reduction originating directly from the formation of inner-sphere complexes on the Stern layer of surface of metal oxides adsorbent.

In our study, the As-O band position of adsorbed species appeared at 803 cm^{-1} and 811 cm^{-1} as a result of the formation of M^{*}–O–As complexes [77]. It is also in agreement with a previous FTIR study of As(V) adsorption on nanocrystalline titanium dioxide [42]. These results indicate that the adsorption process of arsenic on the ATM adsorbent was completed through formation of a surface complex by substituting hydroxyl with arsenic species. That is the pre-dominant mechanism for As(V) adsorption on the ATM.

TGA–DTA analyses of ATM, TM, M, ATM+water and ATM after adsorption of As(III) and As(V) are shown in Fig. S6. The experimental results of thermogravimetric analysis of Ti-Mn binary hydrous oxide (TM) and manganese hydrous oxide (M) in Fig. S6b and Fig. S6c, respectively, confirmed the reference values in [78, 79] that the surface of composites containing Mn-oxides reach the surface state free of -OH group at T_2= 800 °C. Therefore, the TGA-DTA data of all the samples were evaluated in the range of temperature from T_1 =120 °C to T_2 = 800 °C. According to the analyses and results shown in Fig. S6a1 and Table 5, the ATM has a high concentration of surface hydroxyl (125.39 × 10^{20} OH/g) and OH density (D_{OH}, 162.624 OH/nm^2). The D_{OH} is by two orders of magnitude higher than for the other types of binary metal oxides [80, 81]. The concentration of surface hydroxyl of the sample ATM was reduced from 125.39 × 10^{20} OH/g to 112.39 × 10^{20} OH/g after shaking in distilled water and drying at room temperature. The decrease may be caused by the reaction between hydroxyl groups on the ATM surface and H^+ in distilled water. When the blank sample (ATM+water) is compared with ATM samples after interaction with the AS(III) and As(V) in terms of concentration of surface hydroxyl, it is evident that hydroxyl groups were consumed due to the formation of complexes between M*-OH on ATM surface and the As(V) species, involving one or two surface hydroxyl with anion species [82]:

$$M^{*}—OH + L = S\text{-}L^{+} + OH^{-} \quad (7)$$

$$2\,M^{*}—OH + L = 2S\text{-}L^{+} + 2OH^{-} \quad (8)$$

Where M^{*} stands for aluminum, titanium and manganese, L stands for arsenic species.

The density of the hydroxyl groups dropped by 30% due to the adsorption of arsenic species. Interestingly, the addition of Al^{3+} in the synthesis process reduced the specific surface area of Ti-Mn binary hydrous oxide from 336 m^2/g to 71 m^2/g, but it enhanced the number of -OH groups per square unit of ATM surface. Thus, the addition of Al^{3+} resulted in an increase in the -OH groups per gram of adsorbent, leading to an increase in adsorption capacity from 106.4 mg/g, and 54.9 mg/g (TM) (Tab. S3, Fig. S5) to 202.7 mg/g, and 146.7 mg/g (ATM) for As(III) and As(V) at pH7, respectively. The TGA analysis is the simplest method to prove that -OH groups on the ATM surface played an important role in As(III) and As(V) adsorption, which is consistent with the FTIR and XPS analyses.

4. Conclusions

A novel nanosized Al-Ti-Mn trimetal hydrous oxide was synthesized by a facile oxidation and co-precipitation method. Combining the features of single Al, Ti, Mn hydrous oxides, ATM exhibited an *X*-ray amorphous structure with a relatively large BET area (71 m^2/g). The prepared ATM particles are aggregates formed by smaller nanosized particles. The adsorption kinetics and isotherm data were best fitted using the pseudo-second order model and the Langmuir model. The prepared trimetal hydrous oxide exhibited a high adsorption capacity towards both As(V) and As(III), being more effective in As(III) rather than As(V) removal. The maximal adsorption capacities for As(III) and As(V) are 202.7 mg/g, and 146.7 mg/g, at pH 7.0, which outperforms most reported adsorbents. The addition of Al^{3+} in the synthesis process facilitates an increase in the number of M*-OH active sites on the surface of the ATM absorbent, resulting in higher adsorption capacity, which is controlled by the hydroxyl exchange mechanism. Mn-hydrous oxide acted as oxidant ensuring complete conversion of As(III) to As(V) before the adsorption. Due to its excellent arsenic removal performance as well as simple and low-cost synthesis process, the ATM could be a promising adsorbent for both As(III) and As(V) removal from aqueous solutions.

Acknowledgments

The publication is a result of the project Development of the UniCRE Centre (project code LO1606) – "*Green synthesis*", which was financially supported by the Ministry of Education, Youth and Sports of the Czech Republic under the National Programme for Sustainability.

Reference

1. P. L. Smedley and D. G. Kinniburgh, *Applied Geochemistry*, 2002, **17**, 517-568.
2. P. Ravenscroft, H. Brammer and K. Richards, *Arsenic Pollution: A Global Synthesis*, Wiley, 2011.
3. L. Winkel, M. Berg, M. Amini, S. J. Hug and C. Annette Johnson, *Nature Geosci*, 2008, **1**, 536-542.
4. WHO, *Journal*, 2011.
5. *IARC monographs on the evaluation of carcinogenic risks to humans : A Review of Human Carcinogens: Arsenic, Metals, Fibres, and Dusts*, International Agency for Research on Cancer, WHO, Lyon, France, 1987.
6. N. Yamato, *Bulletin of Environmental Contamination and Toxicology*, 1988, **40**, 633-640.
7. M. F. Hughes, L. M. Del Razo and E. M. Kenyon, *Toxicology*, 2000, **143**, 155-166.
8. D. Mohan and J. C. U. Pittman, *Journal of Hazardous Materials*, 2007, **142**, 1-53.
9. B. A. Manning, S. E. Fendorf, B. Bostick and D. L. Suarez, *Environmental Science & Technology*, 2002, **36**, 976-981.
10. S. K. Maji, A. Pal and T. Pal, *Journal of Hazardous Materials*, 2008, **151**, 811-820.
11. R. V. Hedegaard and J. J. Sloth, *Biotechnologie, Agronomie, Société et Environnement*, 2011, **15**, 45.

12. F. Bertolero, G. Pozzi, E. Sabbioni and U. Saffiotti, *Carcinogenesis*, 1987, **8**, 803-808.
13. A. B. Ribeiro, E. P. Mateus and N. Couto, *Electrokinetics Across Disciplines and Continents: New Strategies for Sustainable Development*, Springer International Publishing, 2015.
14. V. Q. Chiu and J. G. Hering, *Environmental Science & Technology*, 2000, **34**, 2029-2034.
15. T. Nishimura and Y. Umetsu, *Hydrometallurgy*, 2001, **62**, 83-92.
16. P. K. Dutta, S. O. Pehkonen, V. K. Sharma and A. K. Ray, *Environmental Science & Technology*, 2005, **39**, 1827-1834.
17. K. Gupta and U. C. Ghosh, *Journal of Hazardous Materials*, 2009, **161**, 884-892.
18. S. Song, A. Lopez-Valdivieso, D. J. Hernandez-Campos, C. Peng, M. G. Monroy-Fernandez and I. Razo-Soto, *Water Research*, 2006, **40**, 364-372.
19. A. Oehmen, R. Valerio, J. Llanos, J. Fradinho, S. Serra, M. A. M. Reis, J. G. Crespo and S. Velizarov, *Separation and Purification Technology*, 2011, **83**, 137-143.
20. D. Nguyen Thanh, M. Singh, P. Ulbrich, N. Strnadova and F. Štěpánek, *Separation and Purification Technology*, 2011, **82**, 93-101.
21. V. K. Sharma and M. Sohn, *Environment International*, 2009, **35**, 743-759.
22. C. A. Martinson and K. J. Reddy, *Journal of Colloid and Interface Science*, 2009, **336**, 406-411.
23. D. N. Thanh, M. Singh, P. Ulbrich, F. Štěpánek and N. Strnadová, *Materials Research Bulletin*, 2012, **47**, 42-50.
24. *Heterogeneous Catalysis of Mixed Oxides: Perovskite and Heteropoly Catalysts*, Elsevier Science, 2013.
25. S. K. Kulshreshtha, M. M. Gadgil and R. Sasikala, *Catalysis Letters*, 1996, **37**, 181-185.
26. G. Zhang, H. Liu, R. Liu and J. Qu, *Journal of Hazardous Materials*, 2009, **168**, 820-825.
27. M. A. Barakat, *Arabian Journal of Chemistry*, 2011, **4**, 361-377.
28. A. Maiti, S. DasGupta, J. K. Basu and S. De, *Separation and Purification Technology*, 2007, **55**, 350-359.
29. L. M. Camacho, R. R. Parra and S. Deng, *Journal of Hazardous Materials*, 2011, **189**, 286-293.
30. K. R. Henke, *Arsenic: environmental chemistry, health threats and waste treatment*, Wiley, 2009.
31. V. Lenoble, C. Laclautre, B. Serpaud, V. Deluchat and J.-C. Bollinger, *Science of The Total Environment*, 2004, **326**, 197-207.
32. Z. Orolínová and A. Mockovciaková, *Materials Chemistry and Physics*, 2009, **114**, 956-961.
33. H. Y. Niu, J. M. Wang, Y. L. Shi, Y. Q. Cai and F. S. Wei, *Microporous and Mesoporous Materials*, 2009, **122**, 28-35.
34. T. Basu and U. C. Ghosh, *Journal of Industrial and Engineering Chemistry*, 2011, **17**, 834-844.
35. G. Zhang, J. Qu, H. Liu, R. Liu and R. Wu, *Water Research*, 2007, **41**, 1921-1928.
36. Z. Li, S. Deng, G. Yu, J. Huang and V. C. Lim, *Chemical Engineering Journal*, 2010, **161**, 106-113.
37. K. Wu, T. Liu, W. Xue and X. Wang, *Chemical Engineering Journal*, 2012, **192**, 343-349.
38. K. Gupta, A. Maity and U. C. Ghosh, *Journal of Hazardous Materials*, 2010, **184**, 832-842.
39. M. A. Ferguson, M. R. Hoffmann and J. G. Hering, *Environmental Science & Technology*, 2005, **39**, 1880-1886.
40. H. Zeng, B. Fisher and D. E. Giammar, *Environmental Science & Technology*, 2007, **42**, 147-152.
41. J. Youngran, M. Fan, J. Van Leeuwen and J. F. Belczyk, *Journal of Environmental Sciences*, 2007, **19**, 910-919.
42. M. Pena, X. Meng, G. P. Korfiatis and C. Jing, *Environmental Science & Technology*, 2006, **40**, 1257-1262.
43. D. G. Kinniburgh, J. K. Syers and M. L. Jackson, *Soil Sci. Soc. Am. J.*, 1975, **39**, 464-470.
44. R. W. M. Kwok, *XPS Peak Fitting Program for WIN95/98 XPSPEAK version 4.1*, 2000.
45. D. A. Shirley, *Physical Review B*, 1972, **5**, 4709-4714.
46. J. H. Scofield, *Journal of Electron Spectroscopy and Related Phenomena*, 1976, **8**, 129-137.
47. Y. S. Ho, J. C. Y. Ng and G. McKay, *Separation Science and Technology*, 2001, **36**, 241-261.
48. P. Ratna Kumar, S. Chaudhari, K. C. Khilar and S. P. Mahajan, *Chemosphere*, 2004, **55**, 1245-1252.

49. A. H. Welch and K. G. Stollenwerk, *Arsenic in Ground Water*, Springer US, 2007.
50. U. C. Ghosh, D. Bandyopadhyay, B. Manna and M. Mandal, *Water Quality Research Journal of Canada*, 2006, **41**, 198-209.
51. M. Singh, D. N. Thanh, P. Ulbrich, N. Strnadová and F. Stepánek, *Journal of Solid State Chemistry*, 2010, **183**, 2979-2986.
52. J. Hlavay and K. Polyák, *Journal of Colloid and Interface Science*, 2005, **284**, 71-77.
53. Z. Xu and X. Meng, *Journal of Hazardous Materials*, 2009, **168**, 747-752.
54. K. Gupta, T. Basu and U. C. Ghosh, *Journal of Chemical & Engineering Data*, 2009, **54**, 2222-2228.
55. T. Wang, W. Yang, T. Song, C. Li, L. Zhang, H. Wang and L. Chai, *RSC Advances*, 2015, **5**, 50011-50018.
56. Z. Ren, G. Zhang and J. Paul Chen, *Journal of Colloid and Interface Science*, 2011, **358**, 230-237.
57. W. Stumm and J. J. Morgan, *Aquatic chemistry: chemical equilibria and rates in natural waters*, Wiley, 1996.
58. Y.-M. Zheng, L. Yu, D. Wu and J. Paul Chen, *Chemical Engineering Journal*, 2012, **188**, 15-22.
59. E. McCafferty and J. P. Wightman, *Surface and Interface Analysis*, 1998, **26**, 549-564.
60. L. V. Duong, B. J. Wood and J. T. Kloprogge, *Materials Letters*, 2005, **59**, 1932-1936.
61. J. F. Moulder and J. Chastain, *Handbook of X-Ray Photoelectron Spectroscopy: A Reference Book of Standard Spectra for Identification and Interpretation of XPS Data*, Perkin-Elmer Corporatioon, Physical Electronics Division, 1992.
62. C. C. Surdu-Bob, S. O. Saied and J. L. Sullivan, *Applied Surface Science*, 2001, **183**, 126-136.
63. H. W. Nesbitt and D. Banerjee, *American Mineralogist*, 1998, **83**, 305-315.
64. M. C. Biesinger, B. P. Payne, A. P. Grosvenor, L. W. M. Lau, A. R. Gerson and R. S. C. Smart, *Applied Surface Science*, 2011, **257**, 2717-2730.
65. G. C. Allen, S. J. Harris, J. A. Jutson and J. M. Dyke, *Applied Surface Science*, 1989, **37**, 111-134.
66. H. W. Nesbitt, G. W. Canning and G. M. Bancroft, *Geochimica et Cosmochimica Acta*, 1998, **62**, 2097-2110.
67. J. S. Foord, R. B. Jackman and G. C. Allen, *Philosophical Magazine A*, 1984, **49**, 657-663.
68. S. Tanuma, C. J. Powell and D. R. Penn, *Surface and Interface Analysis*, 1993, **20**, 77-89.
69. M. J. Scott and J. J. Morgan, *Environmental Science & Technology*, 1996, **30**, 1990-1996.
70. L. Chen, B.-Y. He, S. He, T.-J. Wang, C.-L. Su and Y. Jin, *Powder Technology*, 2012, **227**, 3-8.
71. Y. Zhang, M. Yang and X. Huang, *Chemosphere*, 2003, **51**, 945-952.
72. Y. Zhang, M. Yang, X.-M. Dou, H. He and D.-S. Wang, *Environmental Science & Technology*, 2005, **39**, 7246-7253.
73. K. Nakamoto, *Infrared and Raman spectra of inorganic and coordination compounds*, Wiley, 1978.
74. S. C. B. Myneni, S. J. Traina, G. A. Waychunas and T. J. Logan, *Geochimica et Cosmochimica Acta*, 1998, **62**, 3499-3514.
75. S. C. B. Myneni, S. J. Traina, G. A. Waychunas and T. J. Logan, *Geochimica et Cosmochimica Acta*, 1998, **62**, 3285-3300.
76. B. An and D. Zhao, *Journal of Hazardous Materials*, 2012, **211–212**, 332-341.
77. J. A. Tossell, *Geochimica et Cosmochimica Acta*, 1997, **61**, 1613-1623.
78. R. Mueller, H. K. Kammler, K. Wegner and S. E. Pratsinis, *Langmuir*, 2002, **19**, 160-165.
79. R. A. Lidin, L. L. Andreyeva and V. A. Molochko, *Constants of Inorganic Substances: A Handbook*, Begell House, 1995.
80. M. Chee Kimling, N. Scales, T. L. Hanley and R. A. Caruso, *Environmental Science & Technology*, 2012, **46**, 7913-7920.
81. D. Chen, L. Cao, T. L. Hanley and R. A. Caruso, *Advanced Functional Materials*, 2012, **22**, 1966-1971.
82. W. Stumm, *Aquatic surface chemistry: chemical processes at the particle-water interface*, Wiley, 1987.

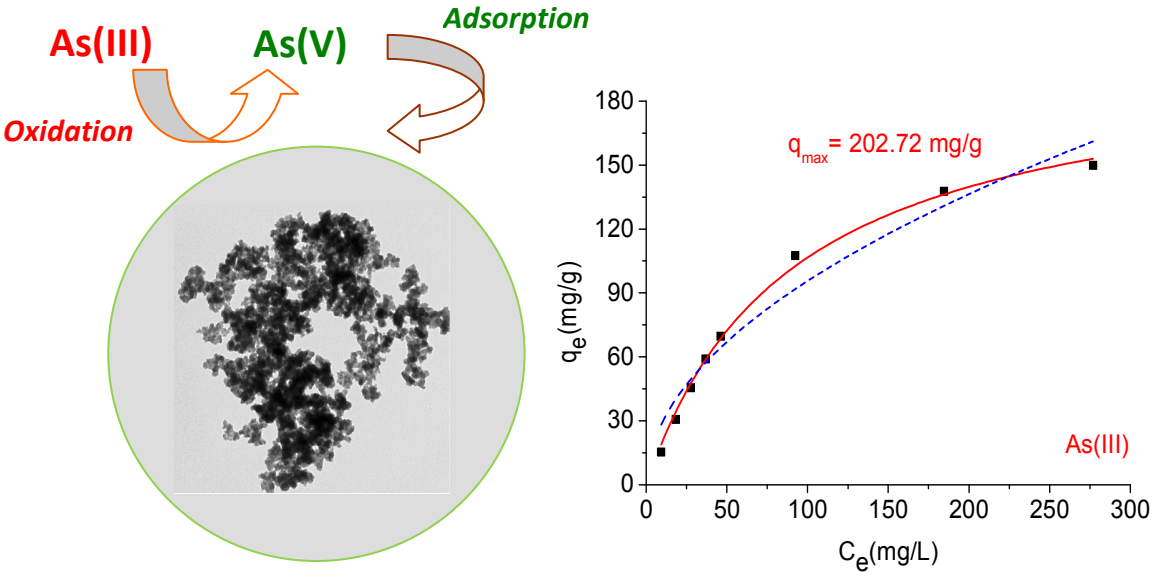

Amorphous nanosized Al-Ti-Mn hydrous oxide